# System Characterization and Polarimetric Calibration of the Ku-Band Advanced Polarimetric Interferometer

Simone Baffelli[*1], Othmar Frey[1,2], Irena Hajnsek[1,3]
[1]Earth Observation & Remote Sensing, ETH Zurich, Switzerland
[2]Gamma Remote Sensing, Gümligen, Switzerland
[3]Microwaves & Radar Institute, Oberpfaffenhofen, German Aerospace Center – DLR, Germany
[*]Email: baffelli@ifu.baug.ethz.ch

## Abstract

This paper addresses the system characterization and the polarimetric calibration of the Ku-Band Advanced Polarimetric Interferometer (KAPRI). KAPRI is an FMCW ground-based real aperture radar system that uses slotted waveguide antennas. The rotation of the antennas introduces undesired phase ramps in azimuth. We present a geometrical model to account for this phase, and propose a method to correct it. Experimental data with a set of trihedral corner reflectors (TCR) in the scene was acquired with the system. A linear phase variation of 30 degrees was observed over the TCR which was geometrically modeled and successfully corrected.

## 1 Introduction

The Ku-Band Advanced Polarimetric Radar Interferometer (KAPRI) is an experimental ground-based FMCW aperture radar (Figure 1). It operates at 17.2 GHz with a chirp bandwidth of 200 MHz, resulting in a range resolution of 0.75 m. Azimuth resolution is obtained by a slotted waveguide antenna with a beamwidth of $0.4°$ (Table 1).
KAPRI is a polarimetric extension of the Gamma Portable Radar Interferometer [1] [1, 2].
In addition to the two standard modes of the GPRI, namely D-INSAR for measurement of line-of-sight displacements and single pass InSAR for digital elevation model generations, using KAPRI it is possible to acquire full polarimetric, interferometric datasets. This is of interest for several applications, especially for the observation of natural targets such as ice, snow or vegetation.
In this paper, we address a number of system-specific effects that have to be modeled and corrected to produce calibrated polarimetric data.

**Table 1:** Summary of the main system characteristics.

| | |
|---|---|
| Center frequency | 17.2 GHz |
| Chrip bandwidth | 200 MHz |
| Chirp duration | variable |
| Range resolution | 0.75 m |
| Antenna length | 2 m |
| Azimuth beamwidth | $0.4°$ |
| Maximum range | approx. 10 km |


**Figure 1:** KAPRI during the first field test. The top two antennas are the H and V polarized transmitting antennas. The four bottom antennas correspond to the two receiving channels, each with a H and a V polarized antenna.

## 2 KAPRI: Data Acquisition and Imaging Procedure

The generation of GPRI/KAPRI data requires the analysis and the correction of several effects, some of them well known from previous experience with the GPRI, others due to the modification to the device and the antennas to permit polarimetric imaging.

### 2.1 Frequency-Dependent Squint

The first effect is encountered at the time of the acquisition of the raw data: to obtain ranging, a chirped signal is transmitted from the antenna. However, in phased-array antennas a deviation of the signal frequency from the design frequency will cause the antenna pattern to squint depending on the frequency, reducing the effective azimuth resolution of the antenna [3]. To overcome this problem, at each frequency bin the dechirped samples are interpolated in azimuth to correct for the frequency-dependent azimuth beam squinting.

After this correction, the raw data is range-compressed using a Fourier transform in range direction [4].

## 2.2 Azimuthal Phase Ramp

Ideally, in a real-aperture radar, the range compressed data can be directly used. However, when the phase of the data is analyzed, an unexpected azimuthal phase ramp is observed. It is presumably caused by the fact that the phase center of the antenna is not positioned at the location of the rotation axis of the radar [5]. In addition, the H and V antennas are not physically identical, such that potentially they have also different phase center locations along the slotted waveguide. We developed a geometrical model to explain this phase artifact and a method to estimate the antenna parameters that fully characterize it. A simple algorithm for the correction of this phase based on a convolution with a suitable matched filter allows us to obtain range-compressed data without azimuth-dependent phase terms.
Once the phase is free of systematic geometrical effects, we can address the polarimetric calibration of the device.
Considering that the system has a very good channel isolato between the receivers and that the acquisition of the polarimetric channels is multiplexed in time, i.e each combination of receiving and transmitting antennas is acquired separately, the crosstalk terms in the polarimetric distortion matrices $\mathbf{R}$ and $\mathbf{T}$ [6] can be assumed to be very small and neglected. Thus, the calibration only requires a trihedral reflector for the correction of the copolar phase and amplitude imbalance. The crosspolar imbalance is estimated using a large number of pixels assumed to be reciprocal [7].

# 3 Scanning-induced Phase Ramp

Consider a real aperture radar with the geometry of Figure 2: an antenna is mounted at the end of a lever arm of length $r_{arm}$. The arm is rotated around the vertical axis at the other end to perform an azimuth scan of the beam. The antenna phase center has an horizontal displacement $r_{ph}$ from the lever arm attachment. This shift is considered in order to model large antennas, where the phase center may be slightly displaced from the mechanical center.
We consider a point scatterer in the scene that has a range of closest approach $r_{sl}$ when the phase center lies on the line connecting the point target to the lever arm rotation center.
Using this geometry, the phase of the signal scattered by the point target and measured at the antenna phase center during the scan can be expressed as a function of the relative rotation from the situation at closest approach, $\theta$:

$$\phi_{pt} = \frac{4\pi}{\lambda} R(\theta) \tag{1}$$

where $R(\theta)$ is the distance from the phase center to the point target.
To compute $R$, we apply the law of cosines on the green triangle in Figure 2: one side has length $c = r_{sl} + r_{ant}$ and the other $r_{ant}$. This length is the equivalent antenna rotation arm for a system with no phase center shift:

$$r_{ant} = \sqrt{r_{arm}^2 + r_{ph}^2}, \tag{2}$$

while the included angle $\theta$ is the rotation from the situation of closest approach:

$$R = \sqrt{c^2 + r_{ant}^2 - 2 c r_{ant} \cos\left(\theta - \theta_c - \alpha\right)}. \tag{3}$$

The function is additionally shifted by the angle $\alpha = \arctan \frac{r_{ph}}{r_{arm}}$. This models the fact that for a displaced phase center the closest approach is not obtained when the target is in the center of the beamwidth. In this case, a faster phase variation is expected because the cosine is steeper in that region.
A real aperture radar with the above described configuration measures the distance $R\left(\theta\right)$ with the associated reflectivity and phase for a series of azimuth positions given by the variable $\theta$. The measured slant range distance depends on the azimuth position of the antenna. Thus range and angle are coupled in the data; this is a form of **R**ange **C**ell **M**igration (**RCM**).
If the range resolution of the system is small enough and the antenna has a small beamwidth, we can assume range and azimuth to be uncoupled because the variation in range induced by the antennas rotation is small enough compared to the range resolution. This means that the response of a point target never leaves the same range bin during the azimuth scan; this is the case for KAPRI. When this approximation is not valid, Equation 3 can be used to compute the range cell migration factor and correct the data.

**Figure 2:** Geometry used for the derivation of the phase. $r_{ph}$: horizontal phase center displacement. $r_{arm}$: antenna lever arm. $\theta$: scan angle of the antenna. $\theta_c$: antenna angle at the closest approach. $r_{sl}$: range of closest approach. $R$ range to the point scatterer during the scan. The antenna beamwidth (gray triangle) is exaggerated.

In the geometrical model the antenna phase center position in the coordinate system centered at the rotation axis is described by two parameters: the length of the antenna lever arm $r_{arm}$ and the horizontal displacement of the phase center along the length of the antenna, $r_{ph}$. The first parameter is specified by the manufacturer, otherwise it is easily measured. This is not the case for $r_{ph}$; if the antenna has a large size and the wavelength is chosen to be small, errors in the manufacturing of the antenna structure can result in significant displacements of the phase center from its intended location at the midpoint of the array. Generally, we determine $r_{ph}$ from the data by solving a nonlinear least squares problem:

$$\underset{(r_{ph}, \phi_{off})}{\operatorname{argmax}} \left|\left|\phi_{meas} - \phi_{sim}\right|\right|^2. \tag{4}$$

Where $\phi_{sim} = \phi_{pt} + \phi_{off}$ is the simulated phase computed using equation 1. A phase offset was added to model the

unknown scattering and propagation phases of the target and the effect of noise. This is necessary in order to compute the correct value for $r_{ph}$, even though the estimated value for the phase offset will not be needed in the phase correction algorithm.

# 4 Methods

## 4.1 Phase Ramp Correction

When the parameter $r_{ph}$ is known, the model in Equation 3 can be used to correct the phase distortion. To do so, for each range distance $r_{sl}$ in the data, the uncorrected azimuth samples are convoluted with a filter of the form:

$$f(\theta) = e^{j\frac{4\pi}{\lambda}R(\theta,r_{sl})} w(\theta). \tag{5}$$

Where $w$ is a windowing function whose length $L_{int}$ should correspond to the beamwidth of the antenna $\theta_{ant}$. In this formula, $R$ is expressed as a function of the distance $r_{sl}$ to make it explicit that the correction is range-variant. The corrected signal is then:

$$d_{corr}(\theta, r_{sl}) = \int_{-\frac{L_{int}}{2}}^{\frac{L_{int}}{2}} e^{j\frac{4\pi}{\lambda}R\left(\theta-\theta', r_{sl}\right)} d(\theta')\, d\theta'. \tag{6}$$

Unlike a synthetic aperture system, the response of a point target in a real aperture radar covers only a very short time in the range-azimuth time domain, because the real antenna aperture is chosen to be as small as possible in order to result in a good azimuth resolution. Thus, real aperture radar system normally do not need azimuth processing and the data in the range-azimuth time domain corresponds to the desired image directly.
For this reason, when convolving the data with an azimuth filter to correct the phase, it is necessary to limit the length of the coherent integration; otherwise samples corresponding to different targets would be combined together, degrading the azimuth resolution and the quality of the phase.

## 4.2 Polarimetric Calibration

In the case of KAPRI, the polarimetric calibration has to be applied after the phase ramp correction. Thus the measured phase only contains scattering and propagation contributions and can be used to derive correct data.
Neglecting crosstalk between the channels, the measured scattering matrix $\mathbf{S_{meas}}$ is assumed to be related to the ideal matrix $\mathbf{S}$ by[7]:

$$\mathbf{S_{meas}} = \begin{bmatrix} S_{hh} & fge^{i(\phi_t)}S_{hv} \\ f/ge^{i(\phi_r)}S_{vh} & f^2e^{i(\phi_r+\phi_t)}S_{vv} \end{bmatrix} \tag{7}$$

where $f$ is the one-way copolarized amplitude imbalance and $g$ the crosspolarized imbalance. $\phi_t = \phi_{t,v} - \phi_{t,h}$ is the phase imbalance when transmitting and $\phi_r = \phi_{r,v} - \phi_{r,h}$ is the receiver phase imbalance. The copolar amplitude imbalance $f$ and $\phi_r + \phi_t$ are determined from the $HH$-$VV$ intensity ratio and the phase difference measured at a corner reflector.
$g$ and $\phi_t - \phi_r$ are estimated from the $HV$-$VH$ amplitude ratio and phase difference averaged over all pixels in the scene. This estimation is based on the assumption of reciprocity for natural distributed targets.
The crosstalk can in first approximation be neglected because of the polarimetric acquisition mode used by KAPRI: only one polarization is acquired at each pulse by connecting the desired transmitting and receiving antennas to the radar electronics using electronic switches.
This method ensures a very high degree of polarization isolato between the channels. The isolation of the receiver has been measured by the manufacturer in the lab by connecting a delay line from the transmitter output to the input port for the $H$ polarized antenna and leaving the $V$ port disconnected. The minimum isolato observed for this configuration is in the order of 40 dB. In this situation, the polarization impurity of the antennas is the only source of crosstalk. Because only the co-polarized antenna pattern is known, it cannot be excluded that a certain amount of crosstalk is caused by the antennas having cross-polarized sidelobes in the direction of copolarized main lobe.
However, as the calibrated data appears to have a good polarimetric quality, the determination and correction of the crosstalk may not be necessary in this case.

# 5 Experimental Data and Results

For the characterization and calibration of KAPRI, a full polarimetric dataset of a scene containing five **T**rihedral **C**orner **R**reflectors (**TCR**) was acquired. The system is equipped with a 2 meters long slotted waveguide antenna with a beamwidth of $0.4°$. The antenna is mounted on a lever arm of length $r_{arm} = 0.25$ m with respect to the vertical rotation axis of the system. During the test, the antenna was rotated in increment of $0.02°$.

## 5.1 Azimuth Phase Ramp

The polarimetric response of the range compressed data was then analyzed; the first step being the computation of the HH-VV phase difference. When examining it, an unexpected phase ramp in azimuth direction was observed at the reflectors. The ramp was mainly caused by a very pronounced linear phase trend in the VV channel (Figure 4). To explain this behavior the geometrical model of chapter section 3 was developed and tested on the TCRs:
The range and azimuth coordinates corresponding to the reflectors were identified and the samples included in the antenna beamwidth where extracted and used to compute $r_{ph}$ with the method described in section 3. The resulting phase center displacement is $r_{ph} = 12$ cm for the VV channel and $r_{ph} = 2$ cm for the HH channel.
The measured and modeled unwrapped phases for one reflector in the VV channel are plotted in Figure 3: we observe a good fit for the azimuthal phase ramp.
Using the estimated value for $r_{ph}$ the data was corrected using Equation 5, with an integration length $L_{int}$ correspond-

ing to $0.7°$. It was observed that a that a longer integration window leads to a better phase response at the cost of a reduced azimuth resolution.

**Figure 3:** Unwrapped azimuthal phase for the TCR, VV channel. The blue line is the measured phase, the green line the phase computed using the model, with an estimated $r_{ph} = 12cm$.

In Figure 4 the oversampled phase and amplitude responses of a TCR for the VV channel are displayed before and after the correction.
In Figure 5 the phase response for all TCRs at the range of maximum intensity is plotted. The phase at the center of the response has been subtracted from the plots for an easier comparison of the azimuthal phase.
The uncorrected data shows an azimuth phase ramp with a variation of approx. $30°$ inside the antenna beamwidth.
The reflectors at 107 and 299 meters have a non-linear response that cannot be explained by the model. The nearer target was presumably not in the full far field region of the radar, that is at approx 500 m. It was likely not illuminated with the full antenna pattern. The corner reflector at 299 m was intentionally partly obscured by a row of trees; its response may contain a contribution by the two way propagation of the beam through the obscuring trees and back to the radar.
In all cases, the phase ramp has been reduced to under $10°$ by the correction. Because of the integration in azimuth, the amplitude response is broadened resulting in a angular resolution of approx $0.7°$.

**(a)** Before phase correction (VV channel).

**(b)** After phase correction (VV channel).

**Figure 4:** Oversampled phase response of a trihedral corner reflector. Range is horizontal, azimuth is vertical. One color cycle corresponds to a phase change of $2\pi$. The intensity is coded in the brightness. The phase at the peak was subtracted.

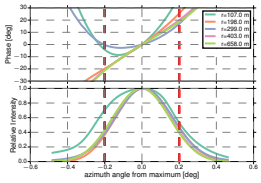


**(a)** Before phase correction.

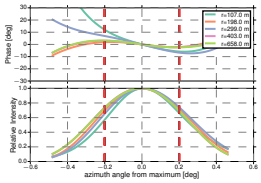


**(b)** After phase correction.

**Figure 5:** Phase and amplitude response for the TCRs. The phase at the maximum has been subtracted to make the two curves comparable. The red lines indicate the width of the antenna beamwidth. The phase variation is under $10°$ after the proposed correction, the residual change being mostly outside of the antenna beamwidth.

## 5.2 Polarimetric Analysis

After the correction of the azimuthal phase ramp, the polarimetric calibration parameters were determined using the procedure described in subsection 4.2. The validity of the polarimetric calibration is verified by computing polarization signatures[8] for the trihedral reflectors. In Figure 6 the co-polarised signatures for two TCRs before and after the calibration are shown. The uncalibrated response is so distorted that it cannot easily be connected with any ideal scattering mechanism. After the phase and imbalance compensation the response is much closer to the expected signature for perfect odd bounce scattering, supporting the validity of the proposed correction and calibration method.

**(a)** Uncalibrated

**(b)** Calibrated

**Figure 6:** Co-polarized signature for two trihedral corner reflectors. Figure 6a before the polarimetric calibration, Figure 6b after the polarimetric calibration procedure.

# 6 Conclusions

In this paper, we addressed aspects of the system characterization required for the full polarimetric calibration of the new ground-based Ku-band interferometric FMCW radar. In particular, we discussed a geometrical model to explain azimuthal phase variation of point target responses in the range-compressed data. An antenna phase center which is displaced with respect to the lever arm is assumed. This induces a slight variation in range during the scan and thus a phase modulation in the phase of point scatterers. This phase

complicates the polarimetric calibration of the device by introducing a phase term unrelated to scattering or propagation in the acquired data.

Using a geometrical model, we can estimate the location of the phase center in the antenna and correct the phase ramp by coherently combining azimuth samples with an appropriate, range-dependent phase correction factor. This produces data where the azimuth phase response of point targets is stable within the 3 dB beamwidth of the antenna. After this correction, a polarimetric calibration technique[7] was applied to correct phase and amplitude imbalances, producing calibrated full polarimetric data. The calibration was verified using the polarization responses of trihedral corner reflectors. The signatures of the corrected data were similar to the expected response for ideal corner reflectors.

# References


[1] C. Werner, A. Wiesmann, T. Strozzi, A. Kos, R. Caduff, U. Wegmuller, and U. Wegmüller, "The GPRI multi-mode differential interferometric radar for ground-based observations," in *EUSAR 2012*. VDE, 2012, pp. 304–307. [Online]. Available: http://ieeexplore.ieee.org/stamp/stamp.jsp?arnumber=06217065

[2] C. Werner, T. Strozzi, A. Wiesmann, and U. Wegmulle, "A real-aperture radar for ground-based differential interferometry," *International Geoscience and Remote Sensing Symposium (IGARSS)*, vol. 3, no. 1, pp. 210–213, jul 2008.

[3] B. Sarkar, R. Roy, and C. Reddy, "Deterioration in resolution of a radar using long slotted waveguide antenna," in *Digest on Antennas and Propagation Society International Symposium*, jun 1989, pp. 1740–1742. [Online]. Available: http://ieeexplore.ieee.org/lpdocs/epic03/wrapper.htm?arnumber=135070

[4] A. Stove, "Linear FMCW radar techniques," *IEE Proceedings F Radar and Signal Processing*, vol. 139, no. 5, p. 343, oct 1992. [Online]. Available: http://digital-library.theiet.org/content/journals/10.1049/ip-f-2.1992.0048

[5] H. Lee, J.-H. Lee, K.-E. Kim, N.-H. Sung, and S.-J. Cho, "Development of a Truck-Mounted Arc-Scanning Synthetic Aperture Radar," *IEEE Transactions on Geoscience and Remote Sensing*, vol. 52, no. 5, pp. 2773–2779, may 2014. [Online]. Available: http://ieeexplore.ieee.org/lpdocs/epic03/wrapper.htm?arnumber=6553134

[6] W. Michael, S. Member, F. T. Ulaby, P. Polatin, and V. V. Liepa, "A General Polarimetric Radar Calibration Technique," *Antennas and Propagation, IEEE Transactions on*, vol. 39, no. 1, pp. 62–67, 1990.

[7] A. G. Fore, B. D. Chapman, B. P. Hawkins, S. Hensley, C. E. Jones, T. R. Michel, and R. J. Muellerschoen, "UAVSAR Polarimetric Calibration," *IEEE Transactions on Geoscience and Remote Sensing*, vol. 53, no. 6, pp. 3481–3491, jun 2015.

[8] J. J. van Zyl, H. A. Zebker, and C. Elachi, "Imaging radar polarization signatures: Theory and observation," *Radio Science*, vol. 22, no. 4, pp. 529–543, 1987. [Online]. Available: http://dx.doi.org/10.1029/RS022i004p00529